Journal of Materials Chemistry A

ROYAL SOCIETY OF CHEMISTRY

PAPER

View Article Online
View Journal | View Issue

Cite this: J. Mater. Chem. A, 2025, 13, 35865

Improved charge transfer performance of eosin Y-sensitized anatase TiO_2 by anchoring group modification: from theoretical design to experiment

Juan Shang,*[abc] Nuttavut Kosem,[ab] Yasuhiro Kayo,[d] Xiao-Feng Shen,[a] Sayo Matsuyama,[a] Motonori Watanabe,[abd] Miki Inada,[a] Tatsumi Ishihara[abd] and Aleksandar Staykov*[ab]

Theoretical design and experimental proof of photocatalytic performance of eosin Y (EY) on anatase TiO_2 with a pyridine linker were obtained for increasing the photobiocatalytic activity of water splitting using visible light. Comparative studies on the hybrid interface of anatase and EY with carboxyl and pyridine anchors were performed by using density functional theory (DFT), time-dependent density functional theory (TD-DFT) calculations and experimental photoreduction of methyl viologen (MV). The geometries, binding interactions between dyes and anatase, electronic structures and electron transfer as well as the effect of isomers (*ortho*, *meta*, and *para*) on the dye/anatase systems were investigated. Theoretical results indicated that EY with carboxyl and pyridine anchors had visible absorption and electron transfer from the dye to the anatase titania. Compared to carboxyl-*para*, which had the best optical performance among carboxyl groups, the adsorption strength of pyridine-*ortho* was close to that of carboxyl-*para*, while the oscillator strength increased significantly, which was more than 10 times higher than that of carboxyl-*para*. Corresponding with the theoretical estimation, EY pyridine linked TiO_2 is active to MV reduction under visible light irradiation by fast charge transfer, in particular, pyridine-*ortho* and *para*. Furthermore, high stability is also achieved for pyridine-*para*. An apparent quantum yield higher than 2.00% and 0.67% under 520 nm light was experimentally achieved in biocatalytic H_2 and NH_3 formation, respectively, for EY pyridine linked TiO_2, which was correctly predicted by the DFT calculations.

Received 15th July 2025
Accepted 16th September 2025

DOI: 10.1039/d5ta05712d

rsc.li/materials-a

1. Introduction

Energy transition, which involves reducing fossil fuel utilization and promoting the development of clean energies, is a crucial issue to mitigate the negative effect of climate change and to pursuit a carbon-neutral society. Hydrogen is considered to be an ideal energy carrier due to its advantages of high specific energy density, purity, versatility, possibilities for renewable production, *etc.*[1,2] As a renewable secondary energy, hydrogen can be generated by many low-carbon-emission pathways such as electrolysis, electro-photolysis, radiolysis, thermo-chemical, *etc.*[3,4] In particular, solar-driven hydrogen production has gained significant attention because it provides a promising opportunity for renewable hydrogen energy, the so-called green hydrogen.

Since the photoelectrolysis method was proposed by Fujishima and Honda in 1972,[5] researchers have steadily increased the attempts to directly harvest solar energy for efficient water electrolysis.[6,7] In photoelectrochemical water splitting systems, photocatalysts which use sunlight energy to dissociate water molecules into hydrogen and oxygen play a key role in the efficiency of hydrogen production.[8,9] Anatase has been one of the most studied photocatalysts because of its appropriate position of the conduction band (CB) edge (lower than the reduction energy of water, 0 V) and valence band (VB) edge (higher than the oxidation energy of oxygen, 1.23 V) to trigger the photoelectrochemical reaction.[8–10] However, the band gap of anatase is *ca.* 3.20 eV which corresponds to ultraviolet (UV) light (only 3–4% of the solar energy).[11] Hence, it is important to narrow the band gap of anatase and to enhance its visible light response and photocatalytic activity.

To date, many modifications have been developed to improve the optical absorption of anatase including dopant

[a]International Institute for Carbon-Neutral Energy Research (WPI-I2CNER), Kyushu University, Motooka 744, Fukuoka, 819-0395, Japan. E-mail: shang.juan.061@m.kyushu-u.ac.jp; alex@i2cner.kyushu-u.ac.jp; Tel: +81-92-802-6717; +81-92-802-6732
[b]Mitsui Chemicals, Inc.-Carbon Neutral Research Center (MCI-CNRC), Kyushu University, Motooka 744, Fukuoka, 819-0395, Japan
[c]The Center for Energy Systems Design (CESD), International Institute for Carbon-neutral Energy Research (WPI-I2CNER), Kyushu University, 819-0395, Japan
[d]Department of Automotive Science, Kyushu University, Motooka 744, Fukuoka, 819-0395, Japan

introduction and dye sensitization. The dopants could be divided into metal and non-metal elements where metals were extensively investigated to act as co-catalysts to increase solar absorption. Some metals such as Au, Pt, Pd, Rh, Ni, *etc.*, have been found to improve the photo electron–hole separation by trapping electrons at the interfaces of metal and anatase.[10,12,13] For example, Murdoch *et al.*[12] found that Au-doped anatase showed a broader visible light absorption range and a high hydrogen production rate. This was because the CB of Au was lower than that of anatase; hence, the excited electrons accumulated at anatase could easily transfer to Au. The hydrogen ions trapped by Au at the interface with anatase enhanced the hydrogen molecule reduction activity. On the other hand, Au, Ni, Cu, Al, Ag, *etc.*, were reported to promote visible light absorption due to the surface plasmon resonance (SPR) effect and localized surface plasmon resonance (LSPR) effect.[9,14–17] These effects could increase the energy intensity of photo-excited electrons under visible light irradiation. Many studies of anatase doping with metal ions, Fe, Mo, Ru, Os, *etc.*, and non-metal anions, N, F, P, S, Si, *etc.*, attempt to modify the inherent bandgap of anatase TiO_2.[10,18–22] Metal ion-doping could form impurity energy levels within the anatase bandgap, while anion-doping could shift the VB upwards and cause a narrowed bandgap of anatase. However, the above methods may have some disadvantages such as the VB shifting upwards could have a detrimental effect on the oxidation activity. Metal-ion dopants may become recombination centers for electrons and holes, which have a negative effect on the photocatalytic water-splitting reaction.[18]

In a previous study, combination of an inorganic photocatalyst with hydrogenase coupled with MV as a redox mediator was studied. The efficiency of hydrogenase genetically formed in *E. coli* is 100% per transferred electron and so the total apparent quantum yield (AQY) of TiO_2/MV^{2+}/hydrogenase in *E. coli* is higher than 30% in the presence of the sacrificial agent of triethanolamine (TEOA). However, TiO_2 can be excited by only UV light (<350 nm). Although a high AQY is achieved, the solar-to-hydrogen efficiency of the photobiocatalytic system using TiO_2 as the inorganic photocatalyst was reduced.[23]

Anchoring of dye-sensitizers to anatase to improve the photocatalytic performance has attracted great attention in recent years. The dye could be excited upon visible light absorption and then excited electrons could transfer from the dye to the CB of anatase. As a result, dye-sensitized anatase can be excited in the visible light region. Organic dyes are currently attracting much interest because of their active visible-light responses, flexible structures, economical and eco-friendliness. Some organic dyes were examined for their light-harvesting capabilities and electron transfer properties such as perylene, cyanine, riboflavin, eosin Y (hereafter referred to as EY) and so on.[8,24–27] Among them, EY has been found to be an effective photosensitizer.[30,31] The Raman spectrum of bare anatase and EY adsorbed TiO_2 indicated that EY could effectively improve the intensity and the range of light absorption on anatase.[29] The EY-sensitized anatase also exhibited a high photo energy conversion efficiency. This is mainly because of the strong ester linkage formed between the carboxyl anchoring group of EY and anatase, which allows efficient electron injection from EY to anatase. However, this linkage was not stable in water due to hydrolysis and easily desorbed from TiO_2 and deactivated.[8,30]

The anchoring group has been confirmed to influence the interaction between dyes and substrates. Several experimental and theoretical studies reported that phosphonic acid is a potential alternative anchoring group.[28–30] It has a strong binding interaction with anatase, showing better long-term stability. Compared to the carboxylic acid anchors, the most prominent benefit of phosphonic acid is the greater adsorption strength, whereas the electronic properties did not improve significantly. The pyridine group was found to be an efficient anchor for the charge injection from fluorescent dyes to anatase.[31] The coordination bond between the pyridine ring and the Lewis acid site behaved as unique intermolecular charge transfer media. Moreover, the pyridine ring exhibited high adsorption stability in water, enabling it to function effectively over extended periods in water-splitting systems. It is necessary to consider both the binding strength and the electronic properties of the anchoring group in order to design a high-performance water-splitting system. Thus, we proposed the use of a pyridine ring as an anchoring group in place of the conventional carboxyl group to connect the EY and anatase. Since the position of the anchor attached to the molecule plays an important role in electron transfer, the isomer (*ortho*-, *meta*-, and *para*-) effect was considered in our theoretical study. The structures of the dye EY investigated in this work are illustrated in Fig. 1. Comparative studies on the hybrid interfaces of anatase and eosin Y with the different anchoring groups were performed by DFT and TD-DFT calculations. The geometries, binding interactions between dyes and anatase, electronic structures and electron transfer as well as the isomer effect on the dye/$Ti_{78}O_{160}H_8$ clusters were investigated and discussed. In addition, electron transport calculations were conducted using non-equilibrium Green's function at the DFT level of theory (NEGF-DFT) on the pyridine-based and the carboxyl-based molecular junctions.

Synthesis of modified eosin Y was performed by using bromobenzaldehyde and pyridin-4-ylboronic acid with a catalytic amount of tetrakis(triphenylphosphine)palladium. Dye-sensitized TiO_2 (dye/TiO_2) as a photocatalytic material was prepared. Photocatalytic reduction of methyl viologen was performed to determine the light-absorbing capacity of photocatalytic materials. Photobiocatalytic H_2 production of dye/TiO_2 coupled with *E. coli* was performed. Finally, we demonstrated the photobiocatalytic NH_3/H_2 production using dye/TiO_2 coupled with cyanobacteria.

2. Computational and experimental methods

2.1. Computational methods

Geometry optimizations of the isolated EY molecular structures shown in Fig. 1 and their complexes with a charge neutral $Ti_{78}O_{160}H_8$ cluster were performed by the DFT method with the PBE exchange–correlation functional.[32] Based on the optimized

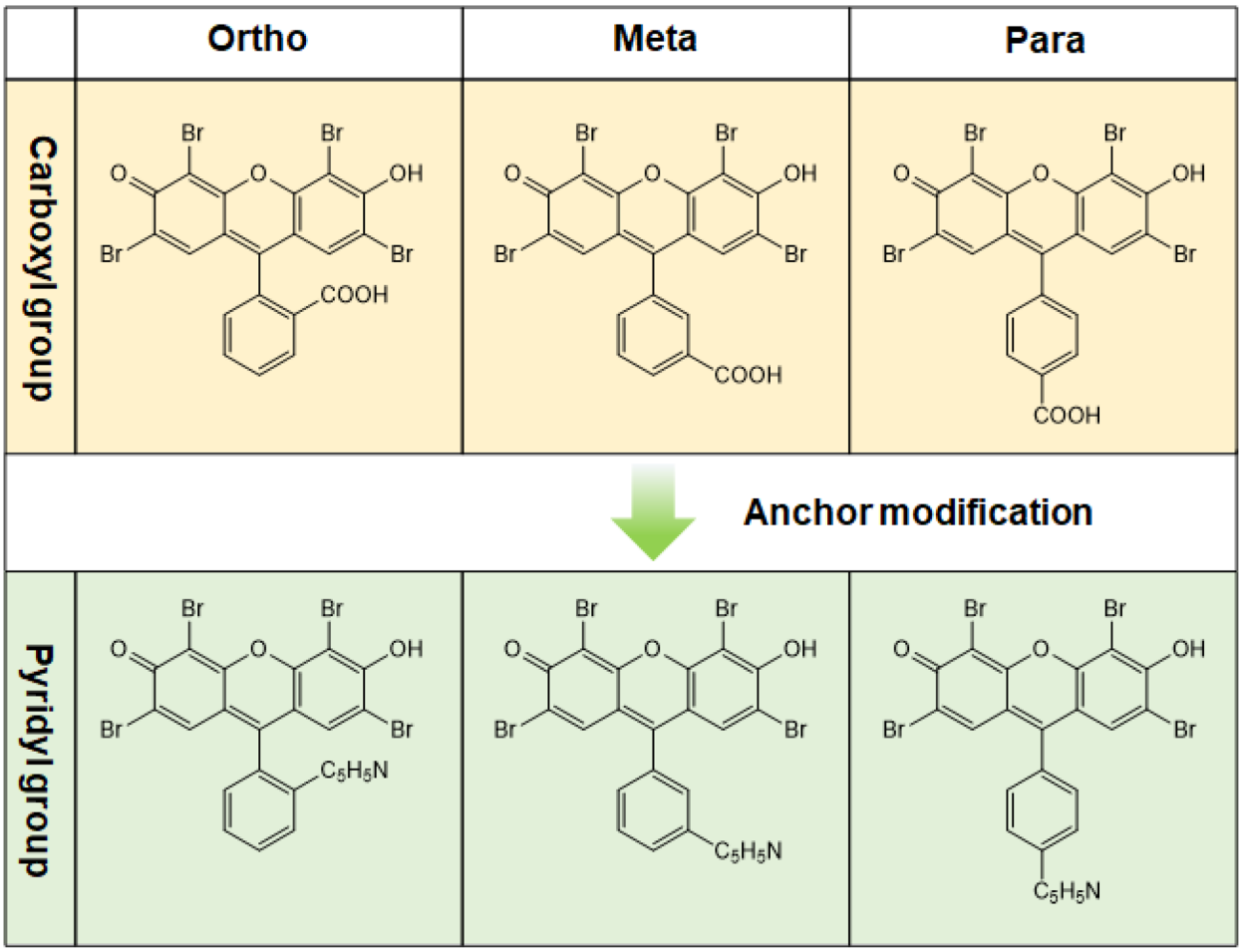

Fig. 1 Molecular structures of the investigated eosin Y isomers anchored with the conventional carboxyl group and modified pyridine group.

structures of dye/anatase, we studied the binding energies (which was the difference between the total energy of dye/anatase, isolated dye and isolated anatase) and the optical properties of the six complexes, by performing TD-DFT calculations with the hybrid B3LYP functional.[33,34] The Karlsruhe def2-SV(P)[35] basis set was applied for all atoms and N-1 Hay–Wadt[36] effective-core potential was employed for the titanium atoms. Based on this method, the optimized lattice properties of anatase crystal were $a = b = 3.78$ Å and $c = 9.51$ Å, close to the experimental values of $a = b = 3.79$ Å and $c = 9.51$ Å.[37] The band gap of anatase calculated using the periodic boundary condition (B3LYP functional and pob-TZVP basis set) was estimated to be 3.28 eV, which was in good agreement with the experimental values of 3.20 eV.[38,39] All the dyes were adsorbed on the fivefold coordinated titanium atoms, which was the Lewis acid site with high reactivity.[33,40] The above calculations were implemented in the Turbomole 7.7 program.[41]

To elucidate the mechanism of enhanced photocatalytic activity of anatase/EY-pyridine, electron transport calculations were performed by the NEGF-DFT method,[42] implemented in the QuantumATK package.[43] Local density approximation (LDA)[44] with the FHI[45] pseudopotential was employed for the calculations. A single zeta-polarized basis set was chosen for the titanium atoms and a double zeta-polarized basis set was chosen for the other atoms.[46] The electric current and transmission spectra at the carboxyl-linked molecular junction and the carboxyl-linked molecular junction, as shown in Fig. 2, were quantitatively investigated in this work. The electrode was modelled by the optimized anatase (001) – (4 × 4) surface with one O–Ti–O layer. For the central scattering region, it was composed of the investigated anchoring group (*i.e.*, carboxyl group and pyridine group), benzene and three layers from each (*i.e.*, three O–Ti–O layers). We used the simplest aromatic hydrocarbon benzene ring as the connection medium to investigate the electric transport through anatase and the different anchors. During the calculations, only the two top O–Ti–O layers as well as the investigated molecules in the scattering region were relaxed, while the two layers on each side in the scattering region and the two electrodes were frozen.

2.2. Synthesis of modified Eosin-Y (EY)

Synthesis of modified eosin Y was performed by using bromobenzaldehyde and pyridin-4-ylboronic acid with a catalytic amount of tetrakis(triphenylphosphine)palladium resulting in the corresponding (pyridin-4-yl)benzaldehyde in 64–94% yields. The obtained products were reacted with resorcinol in

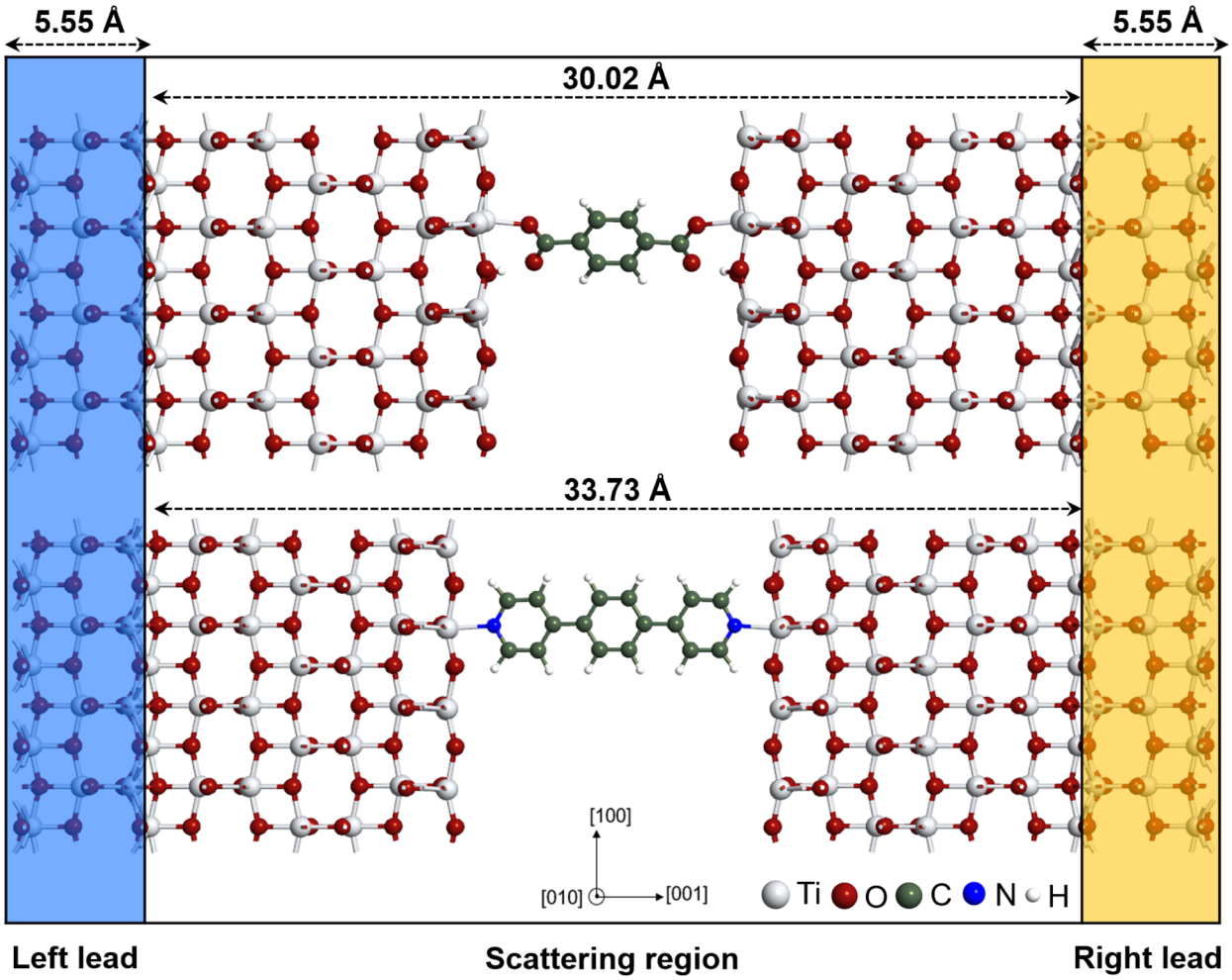

Fig. 2 Structures of the carboxyl-linked device (upper panel) and the pyridine-linked device (lower panel). In all systems, the symmetrical electrodes had a length of 5.55 Å, while the length of the central region in the carboxyl-linked device and the pyridine-linked device was 30.02 Å and 33.73 Å, respectively.

methanesulfonic acid to give fluorescein type derivatives. These obtained compounds were reacted with an excess amount of bromine in ethanol. The precipitated red colored powders were collected to give the corresponding modified eosin Y in 36–42% yields. Thus, the obtained modified products were confirmed using ^{1}HNMR. Details of the synthesis method are mentioned in the SI. ^{1}HNMR analyses showed that the obtained final product is of high purity and does not contain any by-product. ^{1}HNMR was performed with a Bruker AV600 (600 MHz) or a Bruker Avance 400 III HD (400 MHz) spectrometer. The ^{1}H NMR chemical shifts were reported to be δ values (ppm) relative to Me_4Si. The absorption spectra were recorded on a Shimadzu UV-3600. All the solvents and reagents were of reagent quality, purchased commercially, and used without further purification.

2.3. Photocatalytic activity measurement

Photocatalytic reduction of methyl viologen aims to determine the light-absorbing capacity of photocatalytic materials. In principle, photocatalysts can absorb light energy and transfer photoexcited electrons to methyl viologen (MV) as an electron acceptor, facilitating the reduction of oxidized MV^{2+} to reduced $MV^{\bullet+}$. Therefore, measuring the amount of reduced $MV^{\bullet+}$ formed in the reaction directly indicates the capacity of the photocatalysts.

In this work, dye-sensitized TiO_2 (dye/TiO_2) as a photocatalytic material was prepared as follows. The hydrothermal grafting of dye onto the surface of TiO_2 nanoparticles was conducted without any coupling reagents.[47] First, 12.5 mmol of TiO_2 powder (1 g) was dispersed in 60 mL of H_2O using ultrasonication for 5 min, followed by stirring for 30 min to form a homogeneous slurry. Next, 7.5 μmol of dye (approximately 5 mg) was added, and the mixture was stirred for 2 h in the dark to create a dye/TiO_2 suspension. The resulting suspension was then transferred to a Teflon-lined autoclave and heat-treated at 160 °C for 8 h. After cooling to room temperature, the product was collected by centrifugation at 10 000×g for 5 min, thoroughly washed with deionized distilled water to remove any unabsorbed dye molecules and dried at 100 °C under vacuum to obtain dye/TiO_2 nanoparticles.

To determine the visible light-absorbing capacity of dye/TiO_2 nanoparticles, the reaction mixture comprised 100 mM L-cysteine pH 6–8, 1 mg per mL photocatalyst, and 5 mM methyl

viologen (MV^{2+}) solution, with a total reaction volume of 3 mL in a 10 mm × 10 mm quartz cuvette with a screw cap and a polytetrafluoroethylene/silicone septum. Oxygen was displaced by bubbling nitrogen gas through the solution for 2 min. The reaction was initiated by irradiation under visible light using a 300-W Xenon lamp (MAX-303, Asahi Spectra, Japan) equipped with a 520 nm bandpass filter (XBPA520, Asahi Spectra, Japan). At each time point during the reaction, the cuvette was centrifuged at 1000×*g* for 1 min to precipitate the particles that might interfere with absorbance measurements. The reduced $MV^{\bullet+}$ formed during the photocatalytic reaction of dye/TiO_2 was monitored using a UV-vis spectrophotometer (SH-1000Lab, Corona Electric Co., Ltd, Japan) and quantified using a molar absorption coefficient (ε) of 1.3×10^4 M^{-1} cm^{-1}, based on the absorbance value at 605 nm.[48,49] The AQY for photocatalytic $MV^{\bullet+}$ reduction is defined as shown below:[50]

$$\mathrm{AQY}(\%) = 100 \times \frac{\text{Rate of reduced } \mathrm{MV}^{\bullet+}(\mathrm{mol\ s^{-1}})}{\text{Rate of incident photon}(\mathrm{mol\ s^{-1}})}$$

where light intensity at 520 nm is 0.013 W cm^{-2}, irradiation area is 1 cm^2, Avogadro's number is 6.022×10^{23} mol^{-1}, and the rate of incident photons is 0.0562×10^{-6} mol s^{-1}.

2.4. Photobiocatalytic H_2 production of dye/TiO_2 coupled with *E. coli*

The combination of photocatalysts and biocatalysts was carried out according to our previous report[48] with slight modifications for H_2 production. The reaction solution consisted of 100 mM L-cysteine pH 8, 3 mg per mL dye/TiO_2 composite, 5 mM MV^{2+} and 5 mg mL^{-1} recombinant *E. coli* in a quartz reactor with a total volume of 30 mL under anaerobic conditions. After connecting the reactor to a closed gas circulation system linked to a gas chromatograph, the air in the reactor was evacuated and replaced with argon. The reaction was then initiated by irradiation with visible light through a 300-W Xenon lamp equipped with a 520 nm bandpass filter. At each time point, H_2 produced was sampled directly using argon as a carrier gas and monitored by using a gas chromatograph (GC-8A, Shimadzu Corp., Japan) equipped with a molecular sieve 5 A column (GL Sciences Inc., Japan), a thermal conductivity detector at an oven temperature of 50 °C and an integrator (C-R6A, Shimadzu Corp.). The AQY for H_2 production is calculated as shown below:

$$\text{AQY of } \mathrm{H_2}(\%) = 100 \times \frac{2 \times \text{Rate of } \mathrm{H_2}\text{production}(\mathrm{mol\ s^{-1}})}{\text{Rate of incident photon}(\mathrm{mol\ s^{-1}})}$$

where light intensity at 520 nm is 0.013 W cm^{-2}, irradiation area is 1 cm^2, Avogadro's number is 6.022×10^{23} mol^{-1}, and the rate of incident photons is 0.0562×10^{-6} mol s^{-1}.

2.5. Photobiocatalytic NH_3/H_2 production using dye/TiO_2 coupled with cyanobacteria

The combination of photocatalysts and biocatalysts was performed based on our previous report,[49] with slight modifications. Cyanobacterium *Anabaena variabilis* ATCC 29413 was utilized in this study. Cyanobacterial cells were aerobically cultivated in Allen & Arnon medium supplemented with 20 μM Na_2MoO_4 to promote heterocyst differentiation under the light intensity of 5000 Lux (68 μmol m^{-2} s^{-1}) at 26 °C and in a 140 rpm shaking incubator. At a cell density of 1.0 at A_{683} and a chlorophyll a (Chl a) content of ~12 μg mL^{-1}, the cells were harvested by centrifugation at 10 000×*g* for 5 min for experiments. The reaction solution consisted of 100 mM L-cysteine pH 7, 2 mg mL^{-1} of dye/TiO_2 composite, 10 mM MV^{2+} and 50 mg mL^{-1} of cyanobacterial cell mass in a quartz reactor with a total volume of 100 mL under anaerobic conditions. After connecting the reactor to a closed gas circulation system, the reaction was initiated by irradiating it with visible light from a 300-W xenon lamp equipped with a 520 nm bandpass filter.

At each time point, H_2 production and N_2 consumption were monitored using a gas chromatograph (GC-8A, Shimadzu Corp., Japan) equipped with a thermal conductivity detector and an integrator C-R6A (Shimadzu Corp.), with the oven temperature set at 50 °C. The reaction gas was passed through a molecular sieve 5A column (GL Sciences Inc., Japan) using argon as a carrier gas.[48] For NH_3 determination, samples were collected and filtered using Amicon® Ultra-15 Centrifugal Filters-10 K (Merck Millipore) at 5000×*g* for 1 h to remove insoluble components. A 1 mL filtrate was injected into a cation exchange chromatograph (Dionex, USA) equipped with an IonPac™ CG12A (4 × 50 mm) guard column and an IonPac® CS12A (4 × 250 mm) analytical column.[49,51] The concentration of NH_4^+ was calculated using a calibration curve prepared with standard NH_4Cl. The AQY for NH_3 production is calculated as shown below:

$$\text{AQY of } \mathrm{NH_3}(\%) = 100 \times \frac{3 \times \text{Rate of } \mathrm{NH_3}\text{production}(\mathrm{mol\ s^{-1}})}{\text{Rate of incident photon}(\mathrm{mol\ s^{-1}})}$$

where light intensity at 520 nm is 0.013 W cm^{-2}, irradiation area is 1 cm^2, Avogadro's number is 6.022×10^{23} mol^{-1}, and the rate of incident photons is 0.0562×10^{-6} mol s^{-1}.

3. Results and discussion

3.1. Computational design of eosin Y (EY)

Optimized geometries of the EY isomers with the carboxyl and pyridine anchors shown in Fig. 1 adsorbed on the anatase nanoparticle are shown in Fig. 3. Here, we show the magnified views of the adsorption points of the molecules on anatase. Regarding the full structures of the investigated dyes on anatase, the Cartesian coordinates of the complexes can be found in Tables S1–S6, in the SI. EY isomers with the carboxyl anchoring group on the anatase particle were in the H-bonded monodentate adsorption mode with the H atom of the carboxyl group connected to the two-coordinated O atom on the anatase substrate, whereas the pyridine ring adsorbed on the anatase by a sole Ti–N bond. The length of the main electron transport path, Ti–O bond in the anatase/EY-carboxyl, was around 2.15 Å, which was close to that reported previously between anatase and the dyes with the carboxylic acid group, indicating a strong binding interaction between the carboxyl group and anatase.[52,53] This distance was not far from the Ti–N bond connecting the pyridine ring and anatase (in the region of 2.26 Å to 2.28 Å). As can be seen from the calculated binding energies in Fig. 3, EY

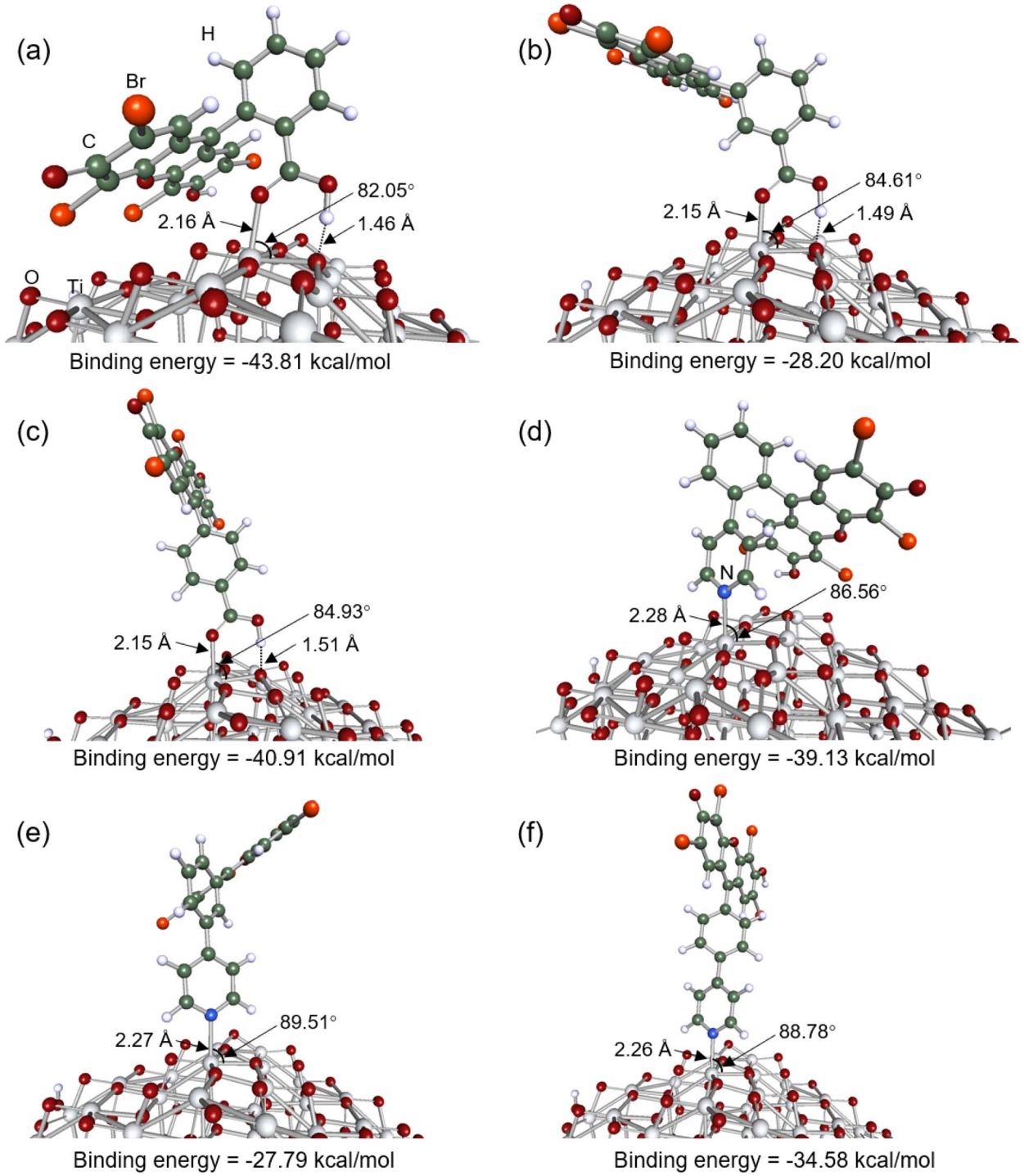

Fig. 3 Optimized geometries and the binding energies of the eosin Y isomers anchored by the carboxyl and pyridine groups on anatase. (a) EY, (b) MEY, (c) PEY, (d) OPyE, (e)MPyE, and (f) PPyE.

isomers anchored by the carboxyl group bind stronger than the corresponding isomers anchored by pyridine to the anatase nanoparticle. The total energies of the isolate dyes, isolate anatase and their combined systems are given in Table S7. On the other hand, the dihedral angles (from 82.05° to 84.93°) formed by the O and Ti atoms of EY-carboxyl/anatase were smaller than those of EY-pyridine/anatase. The smaller dihedral angle could maximize the interaction between the adsorbate and substrate, thus contributing to the high binding energy.[54] Though the EY-pyridine isomers had weaker binding, they show the advantage in stabilization in water compared to the unstable carboxyl group in water due to hydrolysis.[8]

The frontier molecular orbitals of the EY anchored by the carboxyl group and pyridine group are displayed in Fig. 4 and

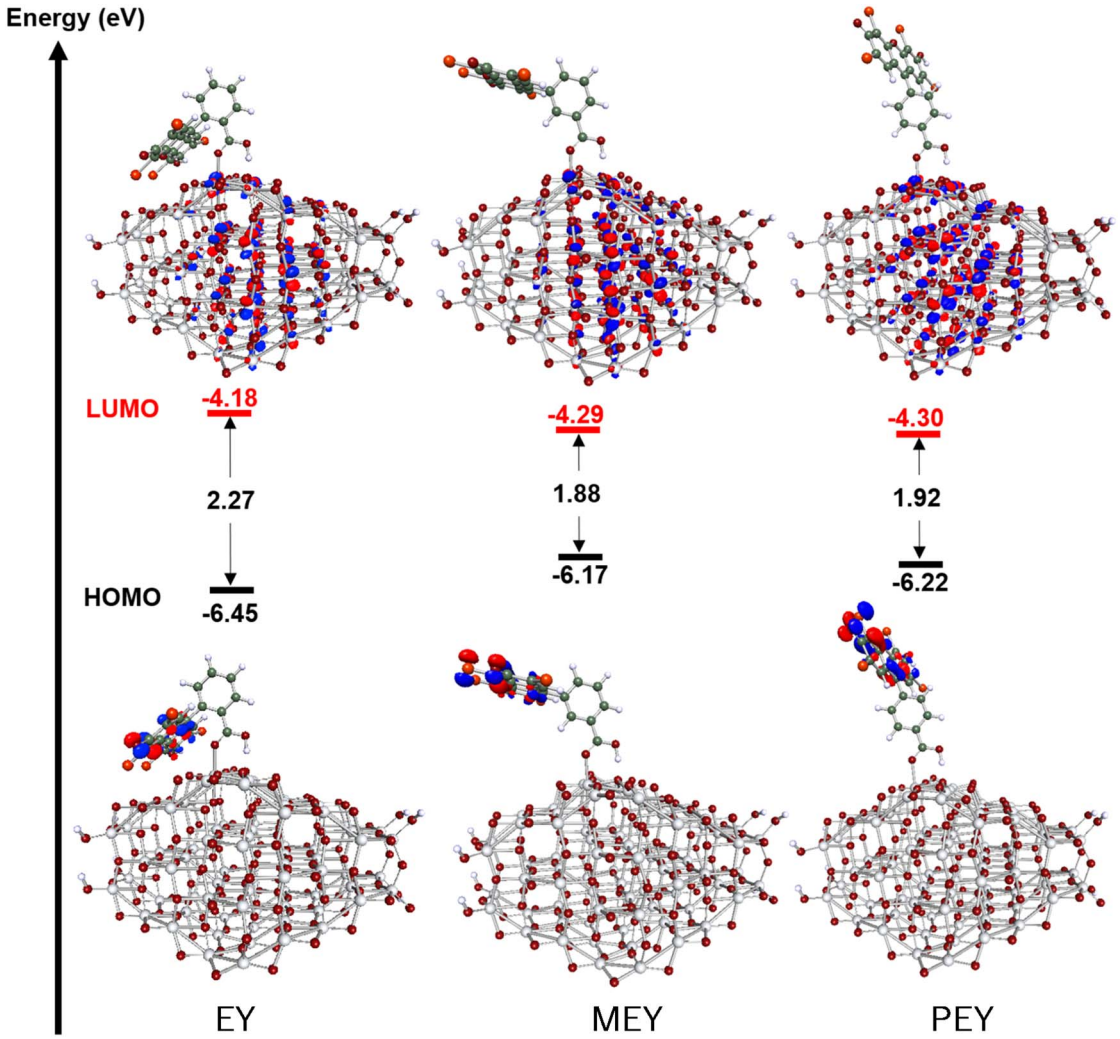

Fig. 4 Frontier orbitals and energy levels of the HOMO and LUMO for the eosin Y isomers anchored by the carboxyl group.

Fig. 5, respectively. The highest occupied molecular orbitals (HOMOs) of all the dyes were delocalized over the three benzene rings and mainly consisted of 2p contributions of the C, Br, and O atoms of the EY.[54] The similar HOMO distributions imply that the modification of the anchoring group for the EY dye retained its molecular character. The lowest unoccupied molecular orbital (LUMO) contributions mainly came from the Ti atoms in the center of anatase nanoparticles. Furthermore, the LUMOs were spatially separated from the HOMOs, which could reduce the probability of electron–hole recombination upon photoexcitation.[55] Similar to the adsorption energy, the HOMO–LUMO gaps of the EY isomers anchored by the carboxyl group were smaller than the corresponding isomers anchored by the pyridine ring. All the linkage types were characterized by a narrow band gap (<2.5 eV), in visible light absorption ranges.

Though all six forms could have visible absorption and electron transfer from the dye to the particle, their UV-vis absorption spectra differed significantly. The wavelengths, oscillator strengths and assignments for the two most probable singlet excitation states are reported in Table 1. The main difference is in the oscillator strength for singlet excitations of the composites, with those linked by the pyridine ring showing the higher photoactivity, compared to those linked by the carboxyl group. The oscillator strength of the anatase sensitized by EY anchored by OPyE was the highest (4.76×10^{-2}) among the investigated complexes, which was 10 times higher than that anchored by PEY (4.44×10^{-3}). The higher transition probability indicates the stronger optical interaction of the designed EY with the anatase particle, as well as the intense transition corresponding to the HOMO → LUMO+1 excitation. At the same time, anatase/OPyE showed a significant advantage in green light absorption, *ca.* 520 nm, whereas a red-shift of the maximum absorption over the range of 606 nm to 655 nm was observed for anatase/PEY. It is worth noting that the difference between the binding energies of anatase/PEY and anatase/OPyE was only 1.78 kcal mol^{-1}. This slight destabilization caused by anchor modification could be masked by the non-negligible optically excited transition. In other words, anatase/OPyE presented unique features in binding interaction, stability in water, electron transfer and light absorption. In addition, there were

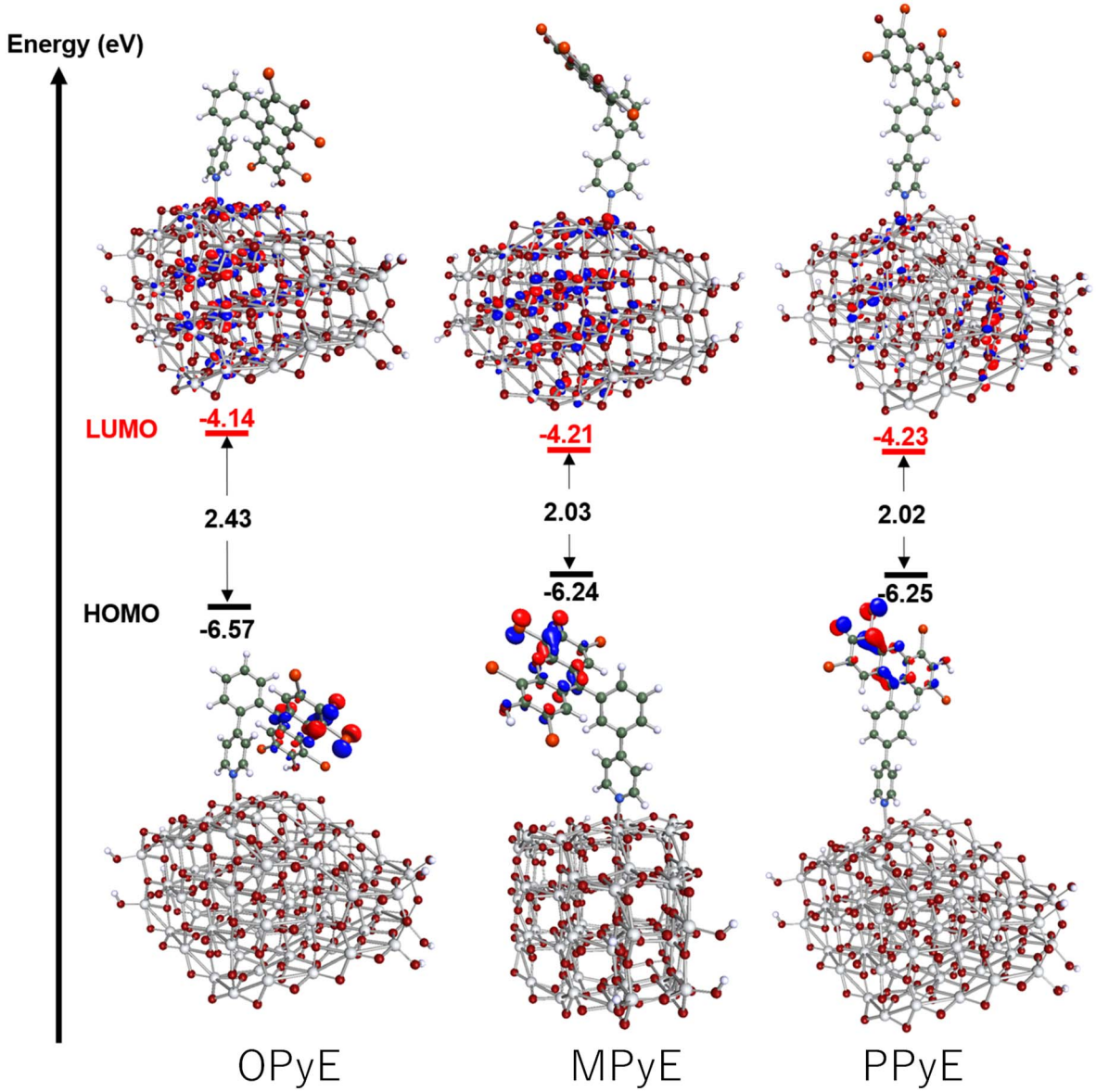

Fig. 5 Frontier orbitals and energy levels of the HOMO and LUMO for the eosin Y isomers anchored by the pyridine group.

two absorption peaks that appeared at 571 nm and 615 nm in the combined system of anatase and PPyE, which were also stronger than those calculated for anatase/PEY. The intense absorption of visible light observed for the anatase/EY-pyridine will have a marked effect on its application in harvesting solar energy photocatalytic systems.

The above results elucidate that modifying the anchoring group to the pyridine ring could significantly improve the photocatalytic performance of anatase. To further understand the electron transfer by the pyridine ring, we examined the electric current in the carboxyl-linked device and the pyridine-linked device, respectively. In the plotted *I–V* curves in Fig. 6a and b, the current increased with the increasing bias voltage for the two devices. In particular, the current increased sharply at the voltage of 1.6 V, where the current in the carboxyl-linked molecular junction was over three orders of magnitude lower than that in the pyridine-linked one. The transmission spectra at 1.6 V bias for the two investigated devices are shown in Fig. 6c and d. Both transmission spectra were characterized by the sharp peak above the Femi level, which originated from the LUMO of the molecules. In the case of the pyridine-based device, two peaks appeared among the bias window of [−0.8 : 0.8] eV at 1.6 V. This indicated that the LUMO served as a conducting channel when the pyridine ring connected to the anatase. Meanwhile, the calculated energy level of the LUMOs for the combined systems of anatase and EY anchored by pyridine (PyE) in Fig. 5 was closer to the Fermi energy compared to the HOMO energy. Thus, it further confirmed that the LUMO dominated the electron transport through the pyridine-connected junction.[56] This was in line with the lower energy positions of LUMOs for the pyridine-linked anatase and EY compared to anatase/EY-carboxyl. The intense resonance

Table 1 Computed excitation properties of the combined systems of anatase and the eosin Y isomers anchored by the carboxyl and pyridine groups. The two most intense singlet excitation states are reported

	Excited state	Wavelength (nm)	Oscillator strength	Transition assignment[a]
Carboxyl-*ortho* (EY)	$S_0 \rightarrow S_1$	635.72	3.20×10^{-5}	H → L (74%), H → L+2 (15%)
	$S_0 \rightarrow S_5$	528.12	1.62×10^{-5}	H → L+8 (33%), H → L+6 (18%)
Carboxyl-*meta* (MEY)	$S_0 \rightarrow S_4$	626.24	4.28×10^{-4}	H → L+3 (81%)
	$S_0 \rightarrow S_1$	736.38	1.78×10^{-4}	H → L (95%)
Carboxyl-*para* (PEY)	$S_0 \rightarrow S_4$	605.68	4.44×10^{-3}	H → L+1 (96%)
	$S_0 \rightarrow S_2$	655.19	1.16×10^{-3}	H → L+3 (92%)
Pyridine-*ortho* (OPyE)	$S_0 \rightarrow S_3$	523.67	4.76×10^{-2}	H → L+1 (42%), H → L+3 (40%)
	$S_0 \rightarrow S_2$	530.39	4.58×10^{-2}	H → L+1 (50%), H → L+3 (28%)
Pyridine-*meta* (MPyE)	$S_0 \rightarrow S_4$	574.62	4.77×10^{-4}	H → L+3 (95%)
	$S_0 \rightarrow S_2$	619.14	1.24×10^{-4}	H → L+1 (97%)
Pyridine-*para* (PPyE)	$S_0 \rightarrow S_4$	571.11	8.05×10^{-3}	H → L+3 (95%)
	$S_0 \rightarrow S_2$	614.73	1.89×10^{-3}	H → L+1 (98%)

[a] Contributions over 15% are displayed. H and L refer to the HOMO and LUMO, respectively.

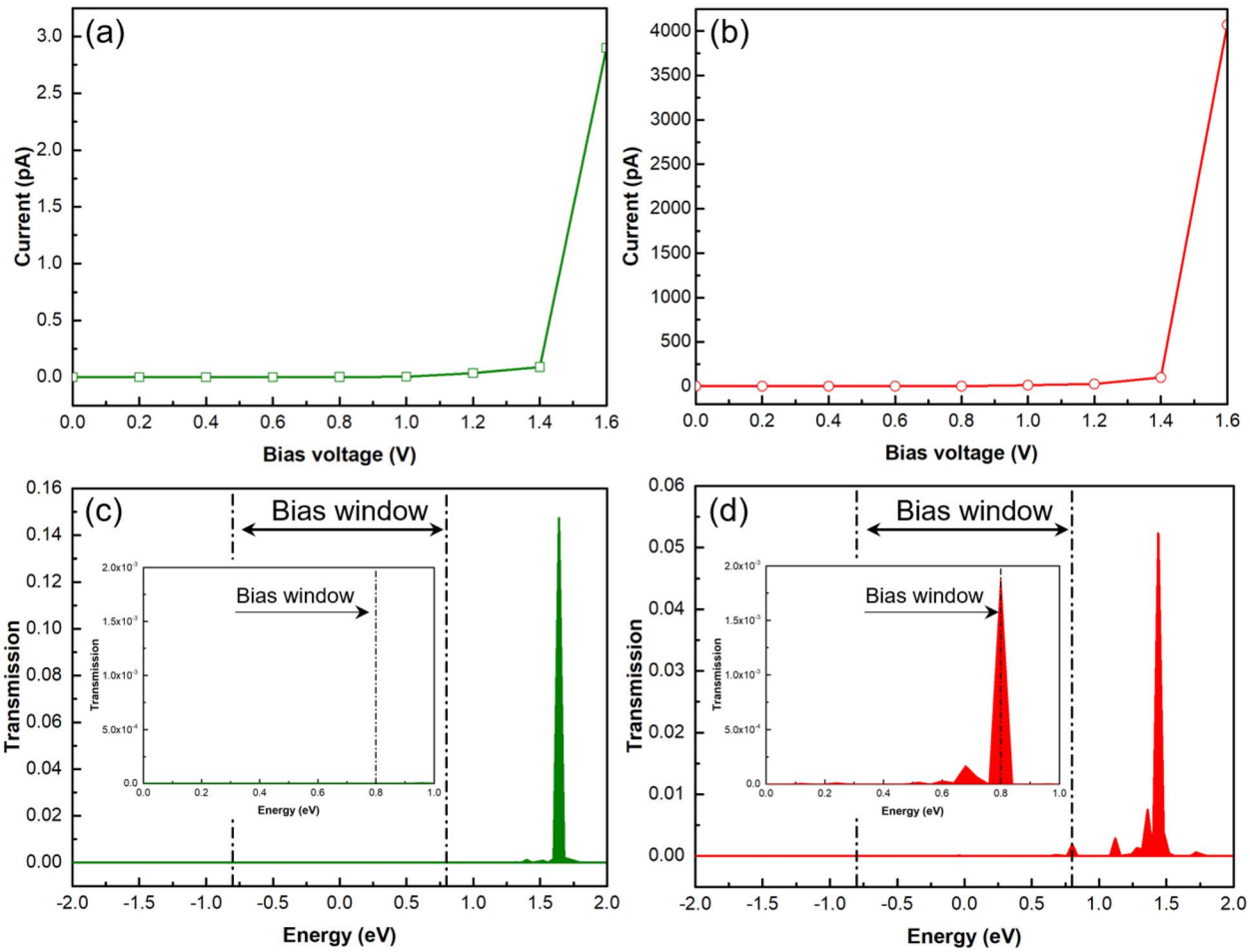

Fig. 6 *I*–*V* curves of (a) the carboxyl-based device as well as (b) the pyridine-based device, and the transmission spectra (c) of the carboxyl-based device as well as (d) the pyridine-based device at 1.6 V bias, where the insets show the magnified spectra around the bias window.

tunneling at high applied biases through the LUMO channel contributed significantly to the high current of the pyridine-based device. The occurrence of a similar electron injection mechanism was found in other pyridine-linked molecular junctions, such as pyridine bridged between two Ag, Au and graphene nanoribbon,[57–59] based on experimental and theoretical studies. The implications of the photocatalytic performance for the pyridine-anchored EY-sensitized anatase are under continuous experimental investigation. Our work provides a design of EY with a pyridine ring to maximize the electron

injection. We performed Mulliken population analysis of representative EY/TiO_2 complexes to quantify interfacial charge redistribution. The results are consistent with our conclusions on electron distribution and interface charge dynamics. In the case of MPyE, it donates $\sim 0.29e^-$ to the $Ti_{78}O_{160}H_8$ cluster, whereas OPyE donates $\sim 0.47e^-$, leading to the higher charge transfer ability of OPyE.

3.2. Photospectroscopic characterization of Eosin Y (EY) on TiO_2

To validate the theoretical calculation suggestions, experimental measurements for the charge transfer from surface modified Eosin Y (EY) to TiO_2 were conducted. Fig. 7 shows the UV-vis absorption spectra of organic dye/TiO_2. A strong absorption peak was observed around 550 nm for all EY modified TiO_2 and this absorption peak is a typical peak of EY. On the other hand, modification of EY shows peaks shift depending on the modified functional group and position. Compared to the pristine EY, carboxyl modified EY shows a higher wavenumber of absorption peak suggesting strong electronic interaction with TiO_2, which is also suggested by DFT calculations. The absorbance of the peak around 520 nm was weak for QPyE, MPyE, and PPyE modified TiO_2 compared with carboxyl EY. This suggests that the molecular photoexcitation coefficient seems to be small for pyridine modified EY. Fig. S1 shows photographs of dye modified TiO_2 and Fig. S1 shows photographs of dye modified TiO_2. Almost the same color is observed; however, in agreement with UV-vis, pyridine modified TiO_2 shows red color. Fig. S2 shows 1 M aqueous solution of modified EY and UV-vis and almost the same order of absorbance with that on TiO_2 shown in Fig. 7a was observed. So, the molecular excitation coefficient changes based on the modified group and PyE has generally a small molecular excitation coefficient. This could be explained by the expansion of the conjugation length caused by the pyridine group.

Photoluminescence spectra are effective for the analysis of the annealing efficiency of photoexcited charge. Photoexcited charge generally recombines with the hole and electron formed, and recombination of charge forms photoluminescence or heat. As shown in Fig. 7b, a broad photoluminescence peak was observed around 600 nm for pristine EY modified TiO_2. On the other hand, the peak intensity decreased in the following order OPyE > MPyE > PPyE > MEY > PEY > EY. This peak intensity represents the charge transfer efficiency and the weaker intensity suggests that photoexcited charge is transferred to the conduction band of TiO_2 more efficiently. Since the molecular excitation efficiency changed, normalized photoluminescence (PL) intensity by UV-vis absorbance is shown in Table S8. The normalized PL intensity is as follows: MPyE > OPyE = EY > PEY > PPyE > MEY, demonstrating that the charge transfer occurs easily on PPyE and MEY which is suggested by theoretical calculations.

The life of photoexcited charge was further studied using transient photoluminescence spectra (Fig. S3 and Table S9 in the SI). Time dependence of the photoluminescence decay period varies with the modified group and its position. In agreement with the order of PL peak intensity shown in Fig. 7b, the PL decay period is also longer. The estimated decay rate for each EY modified TiO_2 is also summarized in Table 2. Since the fast backward reaction shows fast decay of PL, a longer PL for pyridine modified EY (τ = 3.03–3.59 ns) suggests that photoexcited charge has a long life which means photoexcited electrons can transfer to the TiO_2 conduction band and cause charge separation. This long life of photoexcited electrons may be effectively transferred to the active site of the photocatalytic reaction. As predicted by theoretical calculation, *para*-modified pyridine EY shows fast charge transfer to TiO_2.

Table 2 Spectrophotometric measurements of eosin Y and its derivatives

Dye/TiO_2	EY	MEY	PEY	OPyE	MPyE	PPyE
λ_{max} (nm)	527	539	537	544	535	537
Abs (a.u.)	0.83	0.85	0.87	0.29	0.18	0.26
ε (L mol^{-1} cm^{-1})	88 000	79 500	86 350	29 110	17 500	26 490

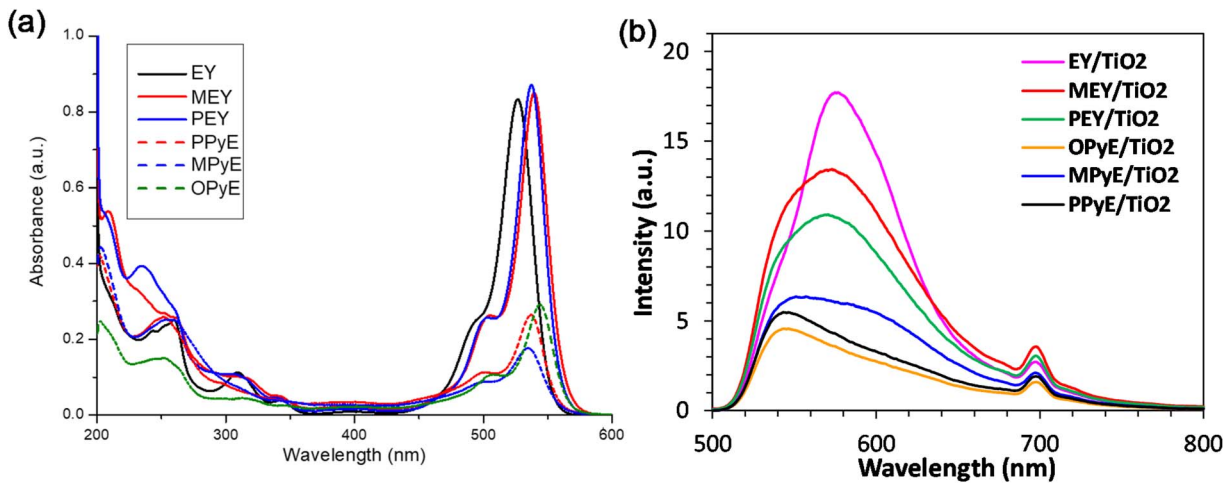

Fig. 7 (a) UV-vis and (b) photoluminescence spectra of dye/TiO_2 nanoparticles.

3.3. Photocatalytic reduction of methyl viologen

The $MV^{\bullet+}$ reduction experiment was performed to demonstrate the transport properties of photoexcited electrons generated by photocatalysts under light illumination. In the photocatalytic $MV^{\bullet+}$ reduction by dye/TiO_2 nanoparticles, L-cysteine was employed as a sacrificial electron donor, dye/TiO_2 composites served as the photocatalytic material, and oxidized methyl viologen (colorless MV^{2+}) acted as an electron acceptor, with its reduced form (dark blue $MV^{\bullet+}$) detectable by spectrophotometry. It was found that no $MV^{\bullet+}$ reduction activity occurred with pure TiO_2, indicating that pure TiO_2 cannot absorb visible light energy to excite electrons. In contrast, the formation of reduced $MV^{\bullet+}$ occurs in the presence of dye on the TiO_2 surface, implying that eosin and its derivatives can absorb light energy at 520 nm to excite electrons to the LUMO level while simultaneously receiving electrons from L-cysteine at the HOMO level. The reaction mechanism of photocatalytic MV^{2+} reduction by dye/TiO_2 in this system can be proposed as follows:

$$\text{L-Cysteine(reduced)} + \text{Dye/TiO}_2 \xrightarrow[520\ \text{nm}]{h\nu} \text{Cystine(oxidized)} + \text{Dye*/TiO}_2 + e^- \quad (1)$$

$$e^- + MV^{2+}\ \text{(colorless)} \rightarrow MV^{\bullet+}\ \text{(blue)} \quad (2)$$

In general, several factors can affect the performance of photocatalysts which should be studied. As shown in Fig. 8a, the effect of pH reveals that carboxyl-eosin/TiO_2 composites exhibit higher activity under acidic conditions, while pyridine-eosin/TiO_2 composites perform better under alkaline conditions. This work reveals the range of optimal pH for each dye/TiO_2 nanoparticle in practical applications. In addition to the pH effect, stability is another key factor to consider. Generally, pure dye molecules dissolved in the reaction solution cannot be reused after experiments. Therefore, dyes anchored on TiO_2 surfaces known as dye/TiO_2 composites have been developed to improve their reusability or more strong bonding. In this study, the reusability of dye/TiO_2 nanoparticles was evaluated based on $MV^{\bullet+}$ reduction activities at pH 8. Each dye/TiO_2 nanoparticle was reused three times for the reaction as shown in Fig. 8b. Among the different photocatalysts, AQY analysis clearly shows that only MPyE/TiO_2 and PPyE/TiO_2 remain stable after three reuse cycles, while the efficiency of other dye/TiO_2 photocatalysts decreased by more than 50%. It is known that dyes bound to the hydroxy site of titanium dioxide by dye-carboxy groups are easily desorbed by hydrolysis in the presence of water.[60,61] Although computer modeling suggests that both carboxyl and pyridine eosin could bind on TiO_2, the experimental results indicate that only MPyE and PPyE are stable on the TiO_2 surface in our reaction system. Although reasonably high photoexcitation properties were achieved for EY without modification, the decrease in activity with time is the most serious drawback; however, MPyE and PPyE show no degradation during recycling. So, in addition to the high efficiency, high stability was achieved by strong bonding of the pyridine group of MPyE and PPyE to TiO_2. Therefore, pyridine-*meta* and pyridine-*para* eosin are the most suitable candidates for further development in future studies.

3.4. Dye-modified TiO_2 in photobiocatalytic H_2 production

To demonstrate the usability of EY modified anatase photocatalytic for H_2 production, we typically combined with a biocatalytic enzyme, hydrogenase, in the photobiocatalytic process. In our system, each dye/TiO_2 nanoparticle serves as a photocatalyst, while a hydrogenase-expressing bacterial cell acts as a biocatalyst in the presence of L-cysteine solution as a sacrificial electron donor and MV^{2+} as an electron mediator

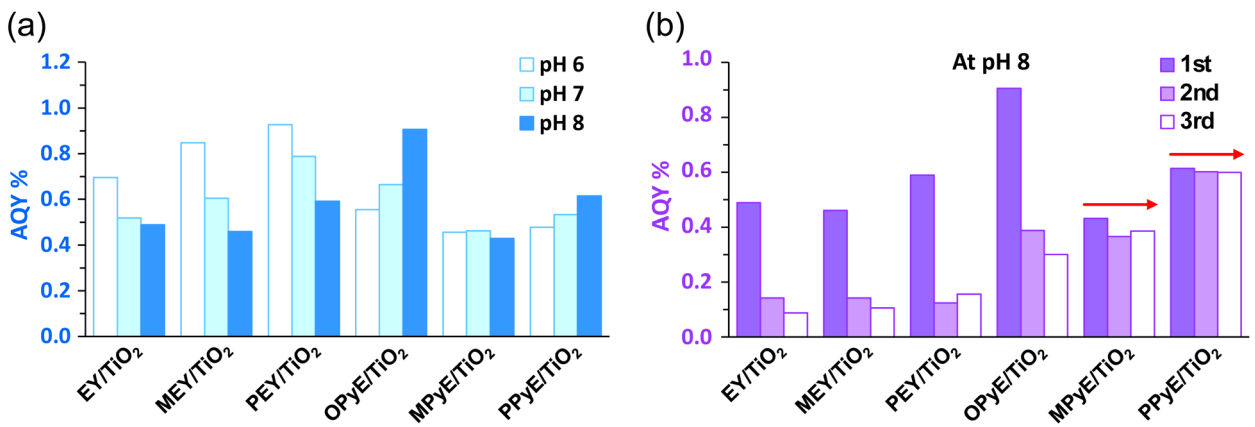

Fig. 8 Methyl viologen ($MV^{\bullet+}$) reduction of different dye/TiO_2 nanoparticles. (a) Effect of pH on $MV^{\bullet+}$ reduction and (b) stability of the nanoparticles in the reaction solution determined by testing their reusability up to three times. The raw data are shown in Fig. S4 and S5.

that transfers photoexcited electrons from the photocatalyst to the biocatalyst for H_2 production.[50] The mechanism of the photobiocatalytic system in this work is illustrated below:

Photocatalytic reaction (light reaction):

$$\text{L-Cysteine(reduced)} + \text{Dye/TiO}_2 + \text{MV}^{2+} \xrightarrow{\frac{h\nu}{520\ \text{nm}}} \text{Cystine(oxidized)} + \text{Dye*/TiO}_2 + \text{MV}^{\cdot+} \quad (3)$$

Biocatalytic reaction (dark reaction):

$$\text{MV}^{\cdot+} + \text{H}^+ \xrightarrow{\frac{\text{Hydrogenase in}}{\text{Recombinant } E.\ coli}} \text{MV}^{2+} + \frac{1}{2}\text{H}_2 \quad (4)$$

According to the results shown in Fig. 9, all dye/TiO_2 composites can be utilized under visible light in the photobiocatalytic system when coupled with hydrogenase-expressing recombinant *E. coli* for H_2 production (Fig. 9a). Among the five different photocatalysts, PPyE/TiO_2 demonstrated the highest activity, achieving an AQY of 1.97%, followed by OPyE/TiO_2, PEY/TiO_2, MPyE/TiO_2, EY/TiO_2, and MEY/TiO_2, respectively, (Fig. 9b) upon the addition of the sacrificial agent. In general, pyridine-eosin/TiO_2 composites exhibit higher efficiency than carboxyl-eosin/TiO_2 composites corresponding to their photocatalytic reduction of MV^{2+}, while pure TiO_2 cannot absorb light energy at 520 nm for H_2 production. This indicates that dye-sensitized molecules on the surface of TiO_2 can absorb visible light energy at 520 nm, generating and transferring photoexcited electrons to the biocatalytic reaction in recombinant *E. coli* for H_2 production. In accordance with prediction, this high AQY was assigned to the efficient charge injection of electrons from the dye to the conduction band of TiO_2. This could be related to the expanded π conjugated orbital.

3.5. Dye-modified TiO_2 in photobiocatalytic NH_3 production

In nature, the ability to synthesize NH_3 is observed in various species of bacteria, archaea, and cyanobacteria under ambient conditions. Nitrogenase is the only biocatalytic enzyme capable of fixing nitrogen by breaking the strong N≡N triple bond of dinitrogen (N_2) gas to NH_3, as shown in eqn (5):[62]

$$\text{N}_2 + 16\text{MgATP} + 8\text{H}^+ + 8\text{e}^- \xrightarrow{\text{[MoFe]-Nitrogenase}} 2\text{NH}_3 + \text{H}_2 + 16\text{MgADP} + 16\text{Pi} \quad (5)$$

Although N_2-fixing microorganisms can produce extracellular NH_3 without generating greenhouse gases or requiring high energy input, nitrogen metabolism in these organisms is tightly regulated to maintain intracellular C–N balance and amino acid pool homeostasis.[63] Due to the low productivity of natural NH_3 synthesis through nitrogenase activity and ATP-dependent photosystem I, the replacement of the photosystem with photocatalysts is the focus of this study.

In the filamentous cyanobacterium *A. variabilis*, nitrogenase is naturally expressed from the *nif* gene cluster within differentiated heterocysts, which function as specialized sites for N_2 reduction.[64] Notably, it has been reported that methyl viologen

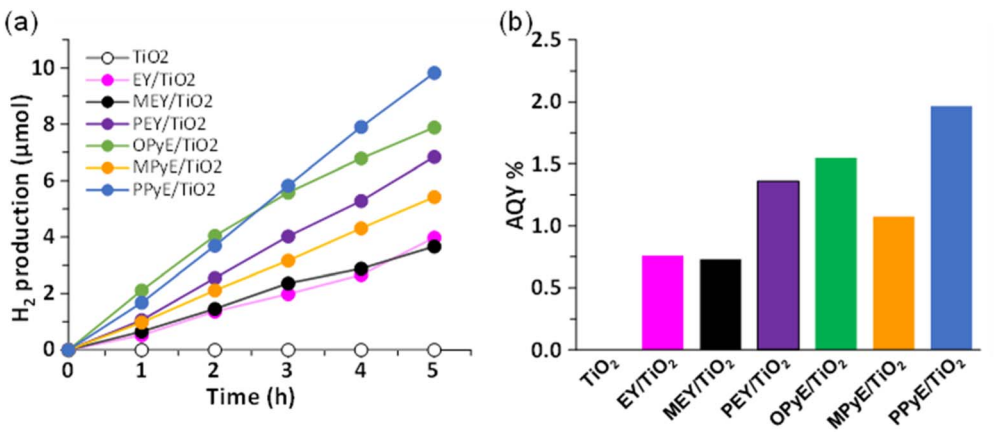

Fig. 9 Photobiocatalytic H_2 production of the dye/TiO_2 composite coupled with recombinant *E. coli* expressing [FeFe]-hydrogenase. (a) A time-course and (b) AQY analysis of H_2 production obtained from the reaction mixture including 100 mM L-cysteine pH 8, 3 mg per mL of the dye/TiO_2 composite, 5 mM MV^{2+} and 5 mg per mL cell mass of recombinant *E. coli* under visible light illumination at 520 nm.

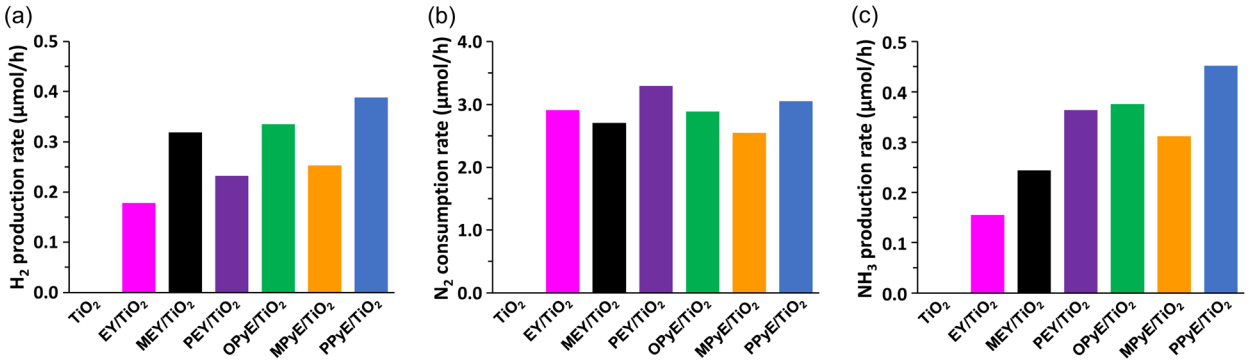

Fig. 10 Rate of (a) H_2 production, (b) N_2 consumption and (c) NH_3 production produced from the photobiocatalytic system of dye/TiO_2 coupled with cyanobacteria in the reaction system including 100 mM L-cysteine pH 7, 2 mg per mL dye/TiO_2, 10 mM MV^{2+} and 50 mg per mL cyanobacterial cell mass under visible light illumination at 520 nm. The raw data are also shown in Fig. S6 and AQY analysis in Table S10.

(MV^{2+}), as an electron mediator, can transfer electrons to nitrogenase, mimicking the natural electron flow through the P-cluster to FeMoco at the enzyme's active site.[65,66] This finding suggests the feasibility of developing an artificial photobiocatalytic system to enhance NH_3 production efficiency under mild conditions.

In this study, dye-modified TiO_2 was applied in a photobiocatalytic system coupled with cyanobacteria *A. variabilis* for NH_3 production in the presence of MV^{2+} and a sacrificial electron donor under visible light (520 nm). During the reaction, the kinetics of H_2 production and N_2 consumption were simultaneously monitored, as shown in Fig. S6 (SI). The rates of NH_3 production, H_2 production, and N_2 consumption are presented in Fig. 10. Among the different dye/TiO_2 composites tested, pyridine-EY/TiO_2 (particularly PPyE/TiO_2 and OPyE/TiO_2) demonstrated higher efficiency in this system, with superior rates and AQY compared to carboxyl-EY/TiO_2, as shown in Table S10 (SI). However, no significant differences were observed in the rates of N_2 consumption.

The results demonstrate that L-cysteine acts as an effective sacrificial reagent, donating electrons to deplete the HOMO level of dye/TiO_2 particles. The excited electrons are transferred to MV^{2+}, reducing it to $MV^{\bullet+}$ during the photocatalytic reaction, which proceeds similarly to the light reaction of H_2 production described in eqn (3). The simultaneous production of NH_3 and H_2, along with N_2 consumption, indicates that the reduced $MV^{\bullet+}$ molecules serve as electron mediators, transferring electrons to cyanobacterial nitrogenase for N_2 reduction and NH_3/H_2 generation under visible light (520 nm). The proposed reaction mechanism for artificial photobiocatalytic NH_3 production using dye/TiO_2 and cyanobacteria is outlined below:

Photocatalytic reaction (light reaction):

$$\text{L-Cysteine(reduced)} + \text{Dye/TiO}_2 + \text{MV}^{2+} \xrightarrow[520\ \text{nm}]{h\nu} \text{Cystine(oxidized)} + \text{Dye*/TiO}_2 + \text{MV}^{\bullet+} \quad (6)$$

Biocatalytic reaction (dark reaction):

$$\text{N}_2 + 8\text{MV}^{\bullet+} + 8\text{H}^+ \xrightarrow[\text{in cyanobacteria}]{\text{[MoFe]-Nitrogenase}} 2\text{NH}_3 + \text{H}_2 \quad (7)$$

4. Conclusion

This study explored the possibility of improving the photocatalytic performance of EY/anatase TiO_2 by anchoring modification. Pyridine ring was used to replace the conventional carboxyl group linker. The structures, adsorption strengths, and electron transfer properties for the systems of anatase and EY anchored by the carboxyl and pyridine ring position were investigated through DFT and TD-DFT calculations and confirmed with experimental support. The adsorption of EY with the carboxyl acid was found to be much stronger than that with the pyridine ring, irrespective of the anchor positions (*ortho*, *para*, and *meta*). While pyridine-linked EY and anatase showed prominent optical properties, the calculated oscillator strength of anatase/EY with pyridine-*ortho* was the highest among the six investigated systems, which was over ten times higher than that with carboxyl-*para* (the highest form among carboxyl anchors). NEGF-DFT calculations were used to elucidate the electron transport in the pyridine-based device and the carboxyl-based device. It was found that the electric current in the pyridine-based device was higher compared to that in the carboxyl-based device. In the case of the pyridine-based device, the transmission spectra at the applied bias showed that two peaks entered the bias window due to the strong electron transfer in the conducting channel, contributing to the high oscillator strength and enhanced catalytic activity. The results imply the promising design of utilizing a pyridine anchor for

the EY/anatase cluster compared to the carboxyl anchor. Experimental validations support this design strategy in good agreement. In particular, by modifying TiO_2 with *para* pyridine MY, AQY for H_2 and NH_3 formation under irradiation of 520 nm visible light was achieved to be *ca.* 2 and 0.67% upon the addition of the sacrificial agent, respectively. No decrease in activity over three times repetition suggests that the pyridine linker is effective not only for charge transfer but also for stable adsorption on anatase. This study demonstrated that molecular design for dye modification by DFT and NEGT-DFT calculation is highly efficient and effective for finding new organic dyes with more efficient charge transfer.

Conflicts of interest

The authors declare no competing financial interest.

Data availability

All data are available upon request from the corresponding author.

Supplementary information: atomic coordinates of the optimized *ortho*, *meta*, and *para* isomers of EY anchored by the carboxyl group as well as pyridine group on anatase, and the total energies of the isolated EY/anatase. See DOI: **https://doi.org/10.1039/d5ta05712d**.

Acknowledgements

This study was financially supported by the Mitsui Chemical Inc Carbon Neutral Research Center (MCI-CNRC). All authors acknowledge the support of the World Premier International Research Center Initiative (WPI), Ministry of Education, Culture, Sports, Science, and Technology of Japan (MEXT).

References

1 M. Yue, H. Lambert, E. Pahon, R. Roche, S. Jemei and D. Hissel, Hydrogen Energy Systems: A Critical Review of Technologies, Applications, Trends and Challenges, *Renew. Sustain. Energy Rev.*, 2021, **146**, 111180.
2 P.-A. Le, V. D. Trung, P. L. Nguyen, T. V. B. Phung, J. Natsuki and T. Natsuki, The Current Status of Hydrogen Energy: An Overview, *RSC Adv.*, 2023, **13**, 28262–28287.
3 F. Dawood, M. Anda and G. M. Shafiullah, Hydrogen Production for Energy: An Overview, *Int. J. Hydrogen Energy*, 2020, **45**, 3847–3869.
4 R. S. El-Emam and H. Özcan, Comprehensive Review on the Techno-Economics of Sustainable Large-Scale Clean Hydrogen Production, *J. Clean. Prod.*, 2019, **220**, 593–609.
5 A. Fujishima and K. Honda, Electrochemical Photolysis of Water at a Semiconductor Electrode, *Nature*, 1972, **238**, 37–38.
6 H. Tong, N. Enomoto, M. Inada, Y. Tanaka and J. Hojo, *Mater. Lett.*, 2015, **141**, 259–262.
7 S. Nishioka, K. Yanagisawa, D. T. Lu, J. J. M. Vequizo, A. Yamakata, K. Kimoto, M. Inada and K. Maeda, *Sustain. Energy Fuels*, 2019, **3**, 2337–2346.
8 R. Abe, K. Hara, K. Sayama, K. Domen and H. Arakawa, Steady Hydrogen Evolution from Water on Eosin Y-Fixed TiO_2 Photocatalyst Using a Silane-Coupling Reagent under Visible Light Irradiation, *J. Photochem. Photobiol., A*, 2000, **137**, 63–69.
9 H. Eidsvåg, S. Bentouba, P. Vajeeston, S. Yohi and D. Velauthapillai, TiO_2 as a Photocatalyst for Water Splitting—An Experimental and Theoretical Review, *Molecules*, 2021, **26**, 1687.
10 C.-H. Liao, C.-W. Huang and J. C. S. Wu, Hydrogen Production from Semiconductor-Based Photocatalysis via Water Splitting, *Catalysts*, 2012, **2**, 490–516.
11 M. Bledowski, L. Wang, A. Ramakrishnan, O. V. Khavryuchenko, V. D. Khavryuchenko, P. C. Ricci, J. Strunk, T. Cremer, C. Kolbeck and R. Beranek, Visible-Light Photocurrent Response of TiO_2–Polyheptazine Hybrids: Evidence for Interfacial Charge-Transfer Absorption, *Phys. Chem. Chem. Phys.*, 2011, **13**, 21511–21519.
12 M. Murdoch, G. I. N. Waterhouse, M. A. Nadeem, J. B. Metson, M. A. Keane, R. F. Howe, J. Llorca and H. Idriss, The Effect of Gold Loading and Particle Size on Photocatalytic Hydrogen Production from Ethanol over Au/TiO_2 Nanoparticles, *Nat. Chem.*, 2011, **3**, 489–492.
13 M. Anpo and M. Takeuchi, The Design and Development of Highly Reactive Titanium Oxide Photocatalysts Operating under Visible Light Irradiation, *J. Catal.*, 2003, **216**, 505–516.
14 Z. Li, L. Shi, D. Franklin, S. Koul, A. Kushima and Y. Yang, Drastic Enhancement of Photoelectrochemical Water Splitting Performance over Plasmonic Al@TiO_2 Heterostructured Nanocavity Arrays, *Nano Energy*, 2018, **51**, 400–407.
15 J. Venturini, F. Bonatto, W. C. Guaglianoni, T. Lemes, S. Arcaro, A. K. Alves and C. P. Bergmann, Cobalt-Doped Titanium Oxide Nanotubes Grown via One-Step Anodization for Water Splitting Applications, *Appl. Surf. Sci.*, 2019, **464**, 351–359.
16 Z. Dong, D. Ding, T. Li and C. Ning, Ni-Doped TiO_2 Nanotubes Photoanode for Enhanced Photoelectrochemical Water Splitting, *Appl. Surf. Sci.*, 2018, **443**, 321–328.
17 S. Y. Sawant, M. S. Sayed, T. H. Han, M. R. Karim, J.-J. Shim and M. H. Cho, Bio-Synthesis of Finely Distributed Ag Nanoparticle-Decorated TiO_2 Nanorods for Sunlight-Induced Photoelectrochemical Water Splitting, *J. Ind. Eng. Chem.*, 2019, **69**, 48–56.
18 W. Choi, A. Termin and M. R. Hoffmann, The Role of Metal Ion Dopants in Quantum-Sized TiO_2: Correlation between Photoreactivity and Charge Carrier Recombination Dynamics, *J. Phys. Chem.*, 2002, **98**, 13669–13679.
19 R. Asahi, T. Morikawa, T. Ohwaki, K. Aoki and Y. Taga, Visible-Light Photocatalysis in Nitrogen-Doped Titanium Oxides, *Science*, 2001, **293**, 269–271.
20 R. Abe, T. Takata, H. Sugihara and K. Domen, Photocatalytic Overall Water Splitting under Visible Light by TaON and

WO_3 with an IO^{3-}/I^- Shuttle Redox Mediator, *Chem. Commun.*, 2005, **30**, 3829–3831.

21 Q. Gao, F. Si, S. Zhang, Y. Fang, X. Chen and S. Yang, Hydrogenated F-Doped TiO_2 for Photocatalytic Hydrogen Evolution and Pollutant Degradation, *Int. J. Hydrogen Energy*, 2019, **44**, 8011–8019.

22 M. H. Elbakkay, W. M. El Rouby, S. I. El-Dek and A. A. Farghali, S-TiO_2/S-Reduced Graphene Oxide for Enhanced Photoelectrochemical Water Splitting, *Appl. Surf. Sci.*, 2018, **439**, 1088–1102.

23 Y. Honda, M. Watanabe, H. Hagiwara, S. Ida and T. Ishihara, Inorganic/Whole-Cell Biohybrid Photocatalyst for Highly Efficient Hydrogen Production from Water, *Appl. Catal., B*, 2017, **210**, 400–406.

24 F. De Angelis, Direct vs. Indirect Injection Mechanisms in Perylene Dye-Sensitized Solar Cells: A DFT/TDDFT Investigation, *Chem. Phys. Lett.*, 2010, **493**, 323–327.

25 W. Chu, K. H. Chan, C. T. Jafvert and Y. S. Chan, Removal of Phenylurea Herbicide Monuron via Riboflavin-Mediated Photosensitization, *Chemosphere*, 2007, **69**, 177–183.

26 C. Chen, X. Qi and B. Zhou, Photosensitization of Colloidal TiO_2 with a Cyanine Dye, *J. Photochem. Photobiol., A*, 1997, **109**, 155–158.

27 M. M. Ibrahim, U. I. Gaya, M. M. Ibrahim and U. I. Gaya, Synthesis of Eosin Y-sensitized Ag-TiO_2 Nano-hybrid for Optimized Photocatalytic Deradation of Aqueous Caffeine, *J. Chil. Chem. Soc.*, 2019, **64**, 4275–4284.

28 P. Wang, Z. Guan, Q. Li and J. Yang, Efficient Visible-Light-Driven Photocatalytic Hydrogen Production from Water by Using Eosin Y-Sensitized Novel g-C_3N_4/Pt/GO Composites, *J. Mater. Sci.*, 2018, **53**, 774–786.

29 (*a*) F. Zhang, F. Shi, W. Ma, F. Gao, Y. Jiao, H. Li, J. Wang, X. Shan, X. Lu and S. Meng, Controlling Adsorption Structure of Eosin Y Dye on Nanocrystalline TiO_2 Films for Improved Photovoltaic Performances, *J. Phys. Chem. C*, 2013, **117**, 14659–14666; (*b*) I. Gillaizeau-Gauthier, F. Odobel, M. Alebbi, R. Argazzi, E. Costa, C. A. Bignozzi, P. Qu and G. J. Meyer, Phosphonate-Based Bipyridine Dyes for Stable Photovoltaic Devices, *Inorg. Chem.*, 2001, **40**, 6073–6079.

30 (*a*) K. Murakoshi, G. Kano, Y. Wada, S. Yanagida, H. Miyazaki, M. Matsumoto and S. Murasawa, Importance of Binding States between Photosensitizing Molecules and the TiO_2 Surface for Efficiency in a Dye-Sensitized Solar Cell, *J. Electroanal.*, 1995, **396**, 27–34; (*b*) S. M. Zakeeruddin, M. K. Nazeeruddin, P. Pechy, F. P. Rotzinger, R. Humphry-Baker, K. Kalyanasundaram, M. Grätzel, V. Shklover and T. Haibach, Molecular Engineering of Photosensitizers for Nanocrystalline Solar Cells: Synthesis and Characterization of Ru Dyes Based on Phosphonated Terpyridines, *Inorg. Chem.*, 1997, **36**, 5937–5946.

31 (*a*) M. Nilsing, S. Lunell, P. Persson and L. Ojamäe, Phosphonic Acid Adsorption at the TiO_2 Anatase (101) Surface Investigated by Periodic Hybrid HF-DFT Computations, *Surf. Sci.*, 2005, **582**, 49–60; (*b*) Y. Ooyama, T. Nagano, S. Inoue, I. Imae, K. Komaguchi, J. Ohshita and Y. Harima, Dye-sensitized Solar Cells Based on Donor-π-acceptor Fluorescent Dyes with a Pyridine Ring as an Electron-withdrawing-injecting Anchoring Group, *Chem.–Eur. J.*, 2011, **17**, 14837–14843.

32 J. P. Perdew, K. Burke and M. Ernzerhof, Generalized, Gradient Approximation Made Simple, *Phys. Rev. Lett.*, 1996, **77**, 3865–3868.

33 A. D. Becke, Density-functional Thermochemistry. I. The Effect of the Exchange-only Gradient Correction, *J. Chem. Phys.*, 1992, **96**, 2155–2160.

34 C. Lee, W. Yang and R. G. Parr, Development of the Colle-Salvetti Correlation-Energy Formula into a Functional of the Electron Density, *Phys. Rev. B: Condens. Matter Mater. Phys.*, 1988, **37**, 785.

35 F. Weigend and R. Ahlrichs, Balanced Basis Sets of Split Valence, Triple Zeta Valence and Quadruple Zeta Valence Quality for H to Rn: Design and Assessment of Accuracy, *Phys. Chem. Chem. Phys.*, 2005, **7**, 3297–3305.

36 P. J. Hay and W. R. Wadt, Ab Initio Effective Core Potentials for Molecular Calculations. Potentials for the Transition Metal Atoms Sc to Hg, *J. Chem. Phys.*, 1985, **82**, 270–283.

37 D. T. Cromer and K. Herrington, The Structures of Anatase and Rutile, *J. Am. Chem. Soc.*, 1955, **77**, 4708–4709.

38 M. Addamo, M. Bellardita, A. Di Paola and L. Palmisano, Preparation and Photoactivity of Nanostructured Anatase, Rutile and Brookite TiO_2 Thin Films, *Chem. Commun.*, 2006, **47**, 4943–4945.

39 Q. Tay, X. Liu, Y. Tang, Z. Jiang, T. C. Sum and Z. Chen, Enhanced Photocatalytic Hydrogen Production with Synergistic Two-Phase Anatase/Brookite TiO2 Nanostructures, *J. Phys. Chem. C*, 2013, **117**, 14973–14982.

40 F. H. Tian, X. Wang, W. Zhao, L. Zhao, T. Chu and S. Yu, Adsorption of 2-Propanol on Anatase TiO_2 (101) and (001) Surfaces: A Density Functional Theory Study, *Surf. Sci.*, 2013, **616**, 76–84.

41 *TURBOMOLE V6.4*, TURBOMOLE GmbH, Karlsruhe, Germany, 2007, **http://www.turbomole.com**.

42 S. Datta, *Quantum Transport: Atom to Transistor*, Cambridge University Press, Cambridge, U.K., 2005.

43 *QuantumATK S-2021.06-SP2; Quantumwise*, Copenhagen, Denmark, 2021, **http://www.quantumwise.com**.

44 W. Kohn and L. J. Sham, Self-Consistent Equations Including Exchange and Correlation Effects, *Phys. Rev.*, 1965, **140**, A1133–A1138.

45 M. Fuchs and M. Scheffler, Ab Initio Pseudopotentials for Electronic Structure Calculations of Poly-Atomic Systems Using Density-Functional Theory, *Comput. Phys. Commun.*, 1999, **119**, 67–98.

46 E. R. Davidson and D. Feller, Basis Set Selection for Molecular Calculations, *Chem. Rev.*, 1986, **86**, 681–696.

47 X. Liu, W. Huang, Y. Lei, Y. Li, Y. Xue, F. Wang and S. Min, Effective Hydrothermal Grafting of Eosin Y onto TiO_2 Nanoparticles Towards Stable Photocatalysts for Efficient Visible-Light-Driven Photocatalytic H_2 Evolution, *New J. Chem.*, 2018, **42**, 6631–6635.

48 N. Kosem, M. Watanabe, J. T. Song, A. Takagaki and T. Ishihara, A Comprehensive Study on Rational

Biocatalysts and Individual Components of Photobiocatalytic H_2 Production Systems, *Appl. Catal., A*, 2023, **651**, 119019.

49 N. Kosem, X.-F. Shen, Y. Ohsaki, M. Watanabe, J. T. Song and T. Ishihara, Photobiocatalytic Conversion of Solar Energy to NH_3 from N_2 and H_2O under Ambient Condition, *Appl. Catal., B*, 2024, **342**, 123431.

50 N. Kosem, Y. Honda, M. Watanabe, A. Takagaki, Z. P. Tehrani, F. Haydous, T. Lippert and T. Ishihara, Photobiocatalytic H_2 Evolution of GaN:ZnO and [FeFe]-Hydrogenase Recombinant *Escherichia coli*, *Catal. Sci. Technol.*, 2020, **10**, 4042–4052.

51 H. Hirakawa, M. Hashimoto, Y. Shiraishi and T. Hirai, Photocatalytic Conversion of Nitrogen to Ammonia with Water on Surface Oxygen Vacancies of Titanium Dioxide, *J. Am. Chem. Soc.*, 2017, **139**, 10929–10936.

52 L. Zhang, X. Liu, W. Rao and J. Li, Multilayer Dye Aggregation at Dye/TiO_2 Interface via π-π Stacking and Hydrogen Bond and Its Impact on Solar Cell Performance: A DFT Analysis, *Sci. Rep.*, 2016, **6**, 35893.

53 L. Zhang and J. M. Cole, Adsorption Properties of P-Methyl Red Monomeric-to-Pentameric Dye Aggregates on Anatase (101) Titania Surfaces: First-Principles Calculations of Dye/TiO_2 Photoanode Interfaces for Dye-Sensitized Solar Cells, *ACS Appl. Mater. Interfaces*, 2014, **6**, 15760–15766.

54 F. Labat, I. Ciofini, H. P. Hratchian, M. Frisch, K. Raghavachari and C. Adamo, First Principles Modeling of Eosin-Loaded ZnO Films: A Step toward the Understanding of Dye-Sensitized Solar Cell Performances, *J. Am. Chem. Soc.*, 2009, **131**, 14290–14298.

55 F. De Angelis, C. Di Valentin, S. Fantacci, A. Vittadini and A. Selloni, Theoretical Studies on Anatase and Less Common TiO2 Phases: Bulk, Surfaces, and Nanomaterials, *Chem. Rev.*, 2014, **114**, 9708–9753.

56 Y. Ie, T. Hirose, H. Nakamura, M. Kiguchi, N. Takagi, M. Kawai and Y. Aso, Nature of Electron Transport by Pyridine-Based Tripodal Anchors: Potential for Robust and Conductive Single-Molecule Junctions with Gold Electrodes, *J. Am. Chem. Soc.*, 2011, **133**, 3014–3022.

57 X. Li, L. Cao, H.-L. Li, H. Wan and G. Zhou, Spin-Resolved Transport Properties of a Pyridine-Linked Single Molecule Embedded between Zigzag-Edged Graphene Nanoribbon Electrodes, *J. Phys. Chem. C*, 2016, **120**, 3010–3018.

58 M. Kamenetska, S. Y. Quek, A. C. Whalley, M. L. Steigerwald, H. J. Choi, S. G. Louie, C. Nuckolls, M. S. Hybertsen, J. B. Neaton and L. Venkataraman, Conductance and Geometry of Pyridine-Linked Single-Molecule Junctions, *J. Am. Chem. Soc.*, 2010, **132**, 6817–6821.

59 O. Adak, R. Korytár, A. Y. Joe, F. Evers and L. Venkataraman, Impact of Electrode Density of States on Transport through Pyridine-Linked Single Molecule Junctions, *Nano Lett.*, 2015, **15**, 3716–3722.

60 H.-O. Son, C. Prasittichai, J. E. Mondloch, L. Luo, J. Wu, D. W. Kim, O. K. Farha and J. T. Hupp, Dye Stabilization and Enhanced Photoelectrode Wettability in Water-Based Dye-Sensitized Solar Cells through Post-assembly Atomic Layer Deposition of TiO_2, *J. Am. Chem. Soc.*, 2013, **135**, 11529–11532.

61 J. Willkomm, K. L. Orchard, A. Reynal, E. Pastor, J. R. Durrant and E. Reisner, Dye-Sensitised Semiconductors Modified with Molecular Catalysts for Light-Driven H_2 Production, *Chem. Soc. Rev.*, 2016, **45**, 9–23.

62 C. J. M. van der Ham, M. T. M. Koper and D. G. H. Hetterscheid, Challenges in Reduction of Dinitrogen by Proton and Electron Transfer, *Chem. Soc. Rev.*, 2014, **43**, 5183–5191.

63 M. I. Muro-Pastor and F. J. Florencio, Regulation of Ammonium Assimilation in Cyanobacteria, *Plant Physiol. Biochem.*, 2003, **41**, 595–603.

64 L. Wang, M. Xia, H. Wang, K. Huang, C. Qian, C. T. Maravelias and G. A. Ozin, Greening Ammonia Toward the Solar Ammonia Refinery, *Joule*, 2018, **2**, 1055–1074.

65 D. G. Boucher, E. Carroll, Z. A. Nguyen, R. G. Jadhav, O. Simoska, K. Beaver and S. D. Minteer, Bioelectrocatalytic Synthesis: Concepts and Applications, *Angew. Chem., Int. Ed.*, 2023, **62**, e202307780.

66 K. Sengupta, J. P. Joyce, L. Decamps, L. Kang, R. Bjornsson, O. Rüdiger and S. DeBeer, Investigating the Molybdenum Nitrogenase Mechanistic Cycle Using Spectroelectrochemistry, *J. Am. Chem. Soc.*, 2025, **147**, 2099–2114.

